Sequential Bond Energies of $Cr(CO)_x^+$, $x = 1-6$

Farooq A. Khan, D. E. Clemmer, Richard H. Schultz,† and P. B. Armentrout*

Department of Chemistry, University of Utah, Salt Lake City, Utah 84112

Received: March 26, 1993; In Final Form: May 25, 1993

The sequential bond energies of $Cr(CO)_x^+$, $x = 1-6$, are determined by collision-induced dissociation in a guided ion beam tandem mass spectrometer. Values for the 0 K bond energies (in eV) are determined to be $D(Cr^+-CO) = 0.93 \pm 0.04$, $D[(CO)Cr^+-CO] = 0.98 \pm 0.03$, $D[(CO)_2Cr^+-CO] = 0.56 \pm 0.06$, $D[(CO)_3Cr^+-CO] = 0.53 \pm 0.08$, $D[(CO)_4Cr^+-CO] = 0.64 \pm 0.03$, and $D[(CO)_5Cr^+-CO] = 1.35 \pm 0.08$. The sum of these bond dissociation energies, 4.99 ± 0.14 eV, is in good agreement with literature thermochemistry. The observation that the relative bond strengths vary nonmonotonically with the number of ligands is discussed in terms of spin conservation and ligand field theory. The bond energy for Cr^+-Xe is also determined as 0.7 ± 0.1 eV and compared with values for other transition metal ion rare gas species.

Introduction

Transition metal carbonyl fragments, $M(CO)_x$, are fundamental building blocks in organometallic chemistry.[1,2] The variation in the physical and chemical properties of these species as the degree of ligation is varied around the metal center is of considerable interest but difficult to study. An important element in characterizing these species is the bond dissociation energy (BDE) of *individual* $(CO)_{x-1}M-CO$ bonds in the absence of solvent effects. To this end, a number of gas-phase studies of cationic,[3-5] neutral,[6,7] and anionic[8] species have been carried out. These studies are of interest because they help build a database of accurate thermochemistry of the coordinatively unsaturated $M(CO)_x$ species, and they provide a benchmark against which theoretical models[9,10] of bonding in these compounds can be tested. Further, these studies can provide general insight into how and why thermochemistry changes with variations in ligation.

In a recent study,[3] we demonstrated that guided ion beam mass spectrometry can be employed to obtain accurate sequential BDEs for $Fe(CO)_x^+$ species. In the present work, we apply this technique to obtain sequential BDEs for $Cr(CO)_x^+$ ions. The $Cr(CO)_x^+$ fragment ions have been characterized previously in a number of electron impact ionization and dissociation experiments on $Cr(CO)_6$.[11-15] In these studies, mass spectra at elevated electron energies show that the $Cr(CO)_5^+$, $Cr(CO)_4^+$, and $Cr(CO)_3^+$ fragments have much smaller abundances than the other fragments. This observation suggests that the BDEs for loss of CO from these species are smaller than those for loss of CO from $Cr(CO)_6^+$, $Cr(CO)_2^+$, and $CrCO^+$. This qualitative observation is confirmed by appearance energies (AEs) for the various $Cr(CO)_x^+$ ions (Table I). Of these, the best BDEs presently in the literature appear to be the threshold photoelectron photoionization coincidence (TPEPICO) experiments carried out by Meisels and co-workers.[16]

Unfortunately, there is reason to question the accuracy of all of these studies for the following reasons. First, the BDEs in Table I vary widely from one study to another. Second, the sum of the BDEs in these experiments is substantially in excess of the enthalpy of reaction 1, 5.05 ± 0.09 eV at 0 K (5.23 ± 0.09 eV at 298 K), obtained as discussed in the next section. Third, the experimental BDEs for $CrCO^+$ and $Cr(CO)_2^+$ are well in excess of values from recent high level ab initio calculations[9] (Table I).

$$Cr(CO)_6^+ \rightarrow Cr^+ + 6CO \qquad (1)$$

† Present address: Department of Chemistry, University of California, Berkeley, CA 94720.

The present study was undertaken to resolve these discrepancies, to obtain a self-consistent set of BDEs for $Cr(CO)_x^+$, $x = 1-6$, and to understand the nonmonotonic variation in the sequential bond energies.

Literature Thermochemistry

Calculating an accurate value for the enthalpy of reaction 1, $\Delta_r H°(1)$, requires a knowledge of the heats of formation of each of the species in the reaction. The heats of formation of Cr^+ and CO are well established (Table II). To obtain $\Delta_f H°[Cr(CO)_6^+]$, we need the ionization energy (IE) of $Cr(CO)_6$ and $\Delta_f H°[Cr(CO)_6, g]$, which is the sum of the heats of formation and sublimation of solid $Cr(CO)_6$. The widely used compilation of Cox and Pilcher[17] recommends a value of -257.6 kcal/mol for $\Delta_f H_{298}°[Cr(CO)_6, s]$, measured by Cotton et al. via conventional bomb calorimetry.[18] When the heat of sublimation measured by Cotton et al.,[18] 17.18 kcal/mol, is added to this, we obtain the gas-phase heat of formation, $\Delta_f H_{298}°[Cr(CO)_6, g] = -240.4$ kcal/mol, as reported by Rosenstock et al.[19] In a subsequent study, Connor, Skinner, and Virmani[20] point out that these heats of formation must be accepted with caution because of problems such as incomplete combustion of the metal and the ill-defined nature of the products when conventional bomb calorimetry is used. A critical evaluation by Pilcher, Skinner, and co-workers[21] recommends $\Delta_f H_{298}°[Cr(CO)_6, s] = -234.2 \pm 0.4$ kcal/mol, a weighted mean of values obtained in three different studies, each of which uses different techniques. We take the heat of sublimation to be 17.14 ± 0.10 kcal/mol, as recommended by Pilcher and co-workers[22] and in excellent agreement with the value of Cotton et al.[18] Thus, we obtain a value for $\Delta_f H_{298}°[Cr(CO)_6, g]$ of -217.1 ± 0.4 kcal/mol, essentially the value cited in such critical compilations as Lias et al.[23]

The heats of formation of a polyatomic molecule at 298.15 and 0 K are related as follows:[24]

$$\Delta_f H_0° = \Delta_f H_{298}° + [H_0° - H_{298}°]_{compound} - \sum [H_0° - H_{298}°]_{elements} \qquad (2)$$

where for a nonlinear polyatomic molecule

$$[H_0° - H_T°]_{compound} \approx -4RT - RT\sum u/(e^u - 1) \qquad (3)$$

and $u = h\nu_i/k_B T$. The $4RT$ term in eq 3 has contributions of $3RT/2$ from translation, $3RT/2$ from rotation, and RT from $\Delta PV = \Delta nRT$ for 1 mol of ideal gas. The summation in eq 3 is carried out over the vibrational frequencies of the polyatomic molecule, ν_i. The vibrational frequencies for $Cr(CO)_6$ are given in Table III[25] and lead to an enthalpy contribution of $12.19RT$.

0022-3654/93/2097-7978$04.00/0

TABLE I: Summary of Values for $D[(CO)_{x-1}Cr^+-CO]$ (in eV) at 298 K[a]

species	ref 12	ref 13	ref 15	ref 16	ref 9	this work
Cr^+–CO	1.4(0.2)	1.47(0.3)	1.33(0.05)	1.33(0.15)	0.90	0.95(0.04)
(CO)Cr–CO	1.74(0.3)	1.69(0.2)	1.52(0.06)	1.36(0.16)	0.93	0.98(0.03)
$(CO)_2Cr^+$–CO	0.94(0.25)	0.84(0.2)	1.16(0.05)	0.66(0.19)		0.59(0.06)
$(CO)_3Cr^+$–CO	0.65(0.16)	1.46(0.2)	0.90(0.04)	0.83(0.17)		0.59(0.08)
$(CO)_4Cr^+$–CO	0.80(0.06)	0.69(0.1)	0.60(0.04)	0.22(0.26)		0.69(0.04)
						0.66(0.03)[b]
$(CO)_5Cr^+$–CO	0.99(0.08)	0.47(0.1)	1.43(0.04)	1.49(0.25)		1.63(0.12)
						1.40(0.08)[b]
sum of BDEs[c]	6.52(0.12)	6.62(0.2)	6.94(0.04)	5.89(0.13)		5.43(0.17)
						5.17(0.14)[b]

[a] Uncertainties are reported in parentheses. [b] Values obtained when including the RRKM analysis, see text. [c] The BDE sum from the literature is 5.23 ± 0.09 eV at 298 K, see text.

TABLE II: Literature Thermochemistry (kcal/mol)[a]

species	0 K	298 K
CO	−27.20 ± 0.04	−26.42 ● 0.04
Cr	94.5 ● 1.0	95.0 ± 1.0
Cr^+	250.5 ± 1.0[b]	252.5 ± 1.0[b]
$Cr(CO)_6$	−218.0 ± 0.4[c]	−217.1 ± 0.4[c]
$Cr(CO)_6^+$	−29.1 ± 1.7[d]	−26.7 ± 1.7[d]

[a] Unless otherwise stated, all data in this table are taken from ref 24. Ion heats of formation at 298 K correspond to the thermal electron convention. [b] Calculated by using IE(Cr) = 6.766 69 ± 0.000 04 eV, ref 47. [c] See text and ref 23. [d] Calculated by using IE[$Cr(CO)_6$] = 8.19 ● 0.07 eV, see text.

TABLE III: Frequencies (cm^{-1}) for $Cr(CO)_x^+$ Species[a]

species	CCrC deformn	CrC stretch	CrCO bend	CO stretch
$Cr(CO)_6^+$[b]	68 (3)	381 (1)	364 (3)	2000 (3)
	95 (3)	394 (2)	436 (3)	2018 (2)
	98 (3)	668 (3)	441 (3)	2112 (1)
			511 (3)	
$Cr(CO)_5^+$ (A)[c]	68 (2)	381 (1)	364 (2)	2000 (2)
	95 (2)	394 (2)	436 (2)	2018 (2)
	98 (3)	668 (2)	441 (3)	2112 (1)
			511 (3)	
$Cr(CO)_5^+$ (B)[c]	60 (3)	350 (4)	350 (5)	2000 (4)
	90 (4)	650 (1)	450 (5)	2100 (1)
$Cr(CO)_5^+$ (C)[c]	60 (3)	350 (5)	300 (5)	2000 (4)
	75 (4)		400 (5)	2100 (1)
$Cr(CO)_4^+$ (A)[c]	60 (5)	300 (3)	300 (4)	2200 (4)
		500 (1)	400 (4)	
$Cr(CO)_4^+$ (B)[c]	75 (5)	400 (3)	350 (4)	2100 (4)
		550 (1)	450 (4)	
$Cr(CO)_4^+$ (C)[c]	100 (5)	400 (2)	350 (4)	2100 (4)
		600 (2)	500 (4)	
$Cr(CO)_3^+$ (A)[c]	40 (3)	150 (2)	250 (6)	2300 (3)
		250 (1)		
$Cr(CO)_3^+$ (B)[c]	60 (3)	250 (1)	350 (6)	2300 (3)
		400 (2)		
$Cr(CO)_2^+$[d]	36 (2)	149 (1)	231 (2)	2381 (1)
		225 (1)	254 (2)	2385 (1)
$CrCO^+$[d]		166 (1)	221 (2)	2381 (1)

[a] Degeneracies in parentheses. [b] The vibrational frequencies for $Cr(CO)_6^+$ are assumed to equal those for $Cr(CO)_6$, ref 25. [c] (A), (B) and (C) refer to independent sets of estimated frequencies. [d] Reference 9.

Thus, $[H_0° - H_{298}°]$ for $Cr(CO)_6$ is $-16.19RT = -9.6$ kcal/mol. The enthalpy changes, $[H_0° - H_{298}°]$, of the elements are −0.970, −1.507, and −6.226 kcal/mol for Cr(c), 6C(graphite) and $3O_2$, respectively.[24] Substituting these values in eq 2, we obtain $\Delta_f H_0°$-[$Cr(CO)_6$, g] = −218.0 ± 0.4 kcal/mol.

Finally, we require an accurate value for IE[$Cr(CO)_6$]. This has been measured in electron impact ionization studies at 8.15 ± 0.17,[11] 8.18 ± 0.07,[12] 8.48 ± 0.08,[13] 8.44 ± 0.05,[14] and 8.42 ± 0.03 eV;[15] and in photoionization studies at 8.24 ± 0.07[16] and 8.142 ± 0.017 eV.[26] The latter number is recommended in the compilation of Lias et al.[23] and is corrected approximately for hot bands, although the identification of the 0–0 origin band does not appear to be definitive. (For instance, Lloyd and Schlag[26] note an inflection at 8.24 eV, in good agreement with the IE from Meisels and co-workers.[16]) We therefore take the average of the two photoionization values as the best determination for the ionization energy, 8.19 ± 0.07 eV. Thus, the heat of formation of $Cr(CO)_6^+$ is −29.1 ± 1.7 kcal/mol at 0 K and −26.7 ± 1.7 kcal/mol at 298 K in the thermal electron convention. From the heats of formation listed in Table II, $\Delta_r H°(1)$ is calculated to be 116.4 ± 2.0 kcal/mol (5.05 ± 0.09 eV) at 0 K and 120.7 ± 2.0 kcal/mol (5.23 ± 0.09 eV) at 298 K.

To compare individual bond energies measured here with those determined in the literature, we also need to convert from 0 to 298 K BDEs. Following the same method outlined above, we determine that the BDEs for $(CO)_{x-1}Cr^+$–CO at 298 K are larger than those at 0 K by 0.43, 0.05, 0.77, 1.34, 0.51, and 1.20 kcal/mol for $x = 1$–6, respectively. The vibrational frequencies needed for the unsaturated chromium carbonyls are listed in Table III and determined as specified below.

Experimental Section

General. Complete descriptions of the apparatus and experimental procedures are given elsewhere.[27,28] $Cr(CO)_x^+$ ions are produced as described below. The ions are extracted from the source, accelerated, and focused into a magnetic sector momentum analyzer for mass analysis. Mass-selected ions are slowed to a desired kinetic energy and focused into an octopole ion guide that radially traps the ions. The octopole passes through a static gas cell containing the neutral reactant at relatively low pressures (~0.05–0.3 mTorr). After exiting the gas cell, product and unreacted beam ions drift to the end of the octopole where they are directed into a quadrupole mass filter for mass analysis and then detected. Ion intensities are converted to absolute cross sections as described previously.[27] Absolute uncertainties in cross sections are about ±20%; relative uncertainties are ±5%.

Laboratory ion energies are related to center-of-mass (CM) frame energies by $E(CM) = E(lab)m/(M + m)$, where M and m are the masses of the ion and neutral reactant, respectively. The zero of the absolute energy scale and the full width at half-maximum (fwhm) of the ion beam kinetic energy distribution are determined by using the octopole as a retarding energy analyzer.[27] The absolute uncertainty in the energy scale is ±0.05 eV (lab). The energy distributions are nearly Gaussian with fmhm of 0.25–0.4 eV (lab).

Ion Source. $Cr(CO)_x^+$ ions are created in a flow tube source[28] that uses He as a carrier gas (flow rate = 7000 sccm, resulting in a flow tube pressure of 550 mTorr). As the He enters the flow tube, it is excited and ionized in a microwave discharge. $Cr(CO)_6$ vapor is introduced into the flow tube ~5 cm downstream from the discharge and ionized by charge transfer from He^+ and possibly by Penning ionization with He^*. Enough energy is present in the $Cr(CO)_6^+$ thus formed to cause fragmentation to form $Cr(CO)_x^+$ ions, $x = 1$–5, with sufficient intensities (>10^4 ions/s) for the present experiments. While traversing the 1 m length of the flow tube, the $Cr(CO)_x^+$ ions undergo ~10^5 collisions with the He carrier gas. This environment should thermalize the

internal energy distribution of the ions to 300 K, the temperature of the flow tube. Previous work on a number of systems is consistent with the production of thermalized ions under similar conditions.[3,28-30]

Data Analysis. In our recent study of the CID of $Fe(CO)_x^+$ ions,[3] we examined several systematic effects on deriving accurate thermodynamic information from CID thresholds. These effects include (a) highly excited reactant ions; (b) multiple collisions with Xe; (c) thermal energy of the reactant ions that might contribute to the measured thresholds; and (d) the lifetime of the dissociating ions. Here, we account for possible systematic errors arising from each of these factors as follows.

First, the ions that traverse the 1 m flow tube are very likely thermalized by the $\sim 10^5$ collisions they undergo, such that excess internal excitation is unlikely. As discussed below, this is verified by comparison of the sum of the bond energies measured with the heat of reaction 1. Second, effects due to multiple collisions with Xe are examined by performing the experiments at two or three different Xe gas cell pressures: ~0.30 and 0.05 mTorr for most ions, ~0.25, 0.10 and 0.05 mTorr for $Cr(CO)_5^+$ and $Cr(CO)_6^+$. We find a negligible Xe pressure dependence on the CID thresholds for all ions studied except $Cr(CO)_3^+$ and $Cr(CO)_6^+$. For these two ions, the thresholds obtained at the higher Xe pressures are noticeably lower than those obtained at lower pressures. This pressure effect is eliminated, following a procedure developed previously,[3,31] by linearly extrapolating the cross sections to zero pressure, rigorously single collision conditions. It is these extrapolated cross sections for $Cr(CO)_3^+$ and $Cr(CO)_6^+$ that are then analyzed further.

Third, we showed in our study of $Fe(CO)_x^+$ ions[3] that a very important systematic effect on CID thresholds is the rotational and vibrational energy of the thermalized ions. Because the rotational energy distribution is relatively narrow, we simply add the average rotational energy of the ions (kT = 0.026 eV for linear ions, $CrCO^+$ and $Cr(CO)_2^+$, and $3kT/2$ = 0.039 eV for nonlinear ions at 298 K) to the measured threshold. The vibrational energy of the ions is best handled by explicitly considering the entire distribution of populated vibrational states. The model used to reproduce the experimental cross sections is then given by

$$\sigma(E) = \sigma_0 \sum_i g_i (E + E_{rot} + E_i - E_0)^n / E \qquad (4)$$

where E is the relative collision energy, E_{rot} is the rotational energy of the reactants, E_0 is the reaction threshold at 0 K, and n is an adjustable parameter. The summation is over the vibrational states i having energies E_i and populations g_i, where $\sum g_i = 1$. We assume that the relative reactivity, as reflected by σ_0 and n, is the same for all vibrational states. Details about our implementation of this equation are given elsewhere.[3] Briefly, the Beyer–Swinehart algorithm[32] is used to evaluate the density of the ion vibrational states, and then the relative populations, g_i, are calculated by the appropriate Maxwell–Boltzmann distribution at 300 K.

The vibrational frequencies of $Cr(CO)_x^+$ ions used in our modeling are given in Table III. For $CrCO^+$ and $Cr(CO)_2^+$ ions, we use the vibrational frequencies calculated by Bauschlicher and co-workers.[9] The vibrational frequencies for the remaining ions are not known and are estimated as follows. First, we assume that the vibrational frequencies of $Cr(CO)_6^+$ are identical to those of $Cr(CO)_6$, which are known.[25] A comparison of the vibrational frequencies of $Cr(CO)_6^+$ and $Cr(CO)_2^+$ then reveals that the addition of CO ligands causes the bending and stretching vibrations involving the metal center to have a larger frequency, with a concomitant decrease in the CO vibrational frequency. This allows us to make an educated guess for the vibrational frequencies of $Cr(CO)_3^+$, $Cr(CO)_4^+$, and $Cr(CO)_5^+$ ions. We explicitly consider several possible sets of frequencies where the values chosen for different modes have upper and lower bounds given by those for $Cr(CO)_2^+$ and $Cr(CO)_6^+$. In general, we find that the data analysis is insensitive to the choice of vibrational frequencies, such that the threshold energies vary by less than 10% for the different sets of frequencies listed in Table III.

Finally, we explicitly examine lifetime effects on the thresholds by accounting for ions with energy in excess of the dissociation energy that do *not* dissociate within our experimental time window. The dissociation of $Cr(CO)_x^+$ species must occur during the flight time τ from the gas cell to the quadrupole mass filter that is used for mass analysis. While τ does depend on the kinetic energies of the ions, it is roughly 10^{-4} s (as previously measured by pulsing the ion beam)[27] in the threshold regions of the experiments described here. Dissociation of ions is expected to become increasingly inefficient as the size of the $Cr(CO)_x^+$ species increases because this increases the number of vibrational modes where internal energy can randomize. This lifetime effect is examined by incorporating RRKM theory into eq 4, as discussed in detail in the Appendix.

The only information required to implement this theory is vibrational frequencies for the transition state associated with the dissociation. This choice is reasonably straightforward because the transition state should be fairly loose and similar to the CID products. Thus, most of the frequencies are those of the $Cr(CO)_{x-1}^+$ product and are taken from Table III. The six frequencies lost upon removal of a CO ligand are chosen as follows. One of the Cr–C stretching frequencies is chosen as the reaction coordinate and removed. One of the CO stretching frequencies is changed to the free CO value. Two of the bending frequencies are lowered to 175 cm^{-1} and two of the C–Cr–C deformations are lowered to 50 cm^{-1}. The latter values are those used by Fletcher and Rosenfeld[7] in a study of unimolecular decomposition of $Cr(CO)_6$ and $Cr(CO)_5$.

Before comparison with the experimental data, the model cross section, eqs 4 or A7 of the Appendix, is convoluted over the ion and neutral translational energy distributions, as described previously.[27] The parameters in eqs 4 and A7, σ_0, E_0, and n, are then optimized by using a nonlinear least-squares analysis to best reproduce the data. The optimized value of E_0 is taken to be the measured threshold for a given data set. Uncertainties in the reported thresholds are derived from the spread of E_0 values from different data sets, from data obtained at different pressures (except for $Cr(CO)_3^+$ and $Cr(CO)_6^+$, where only data extrapolated to zero pressure are analyzed), from the uncertainties introduced by the choice of vibrational frequencies of the $Cr(CO)_x^+$ ions, from variation of the time scale for dissociation τ by a factor of 2, from the two possible forms for including the lifetime effect (see the Appendix) and from the absolute error in the energy scale (±0.05 eV in the laboratory frame).

In our analysis of $Cr(CO)_x^+$, x = 3–6, we also use a modified form of eq 4 that accounts for a decline in the product ion cross section at higher kinetic energies. This model has been described in detail previously[33] and depends on E_D, the energy at which a dissociation channel can begin, and p, a parameter similar to n in eq 4.

Results

Collision-induced dissociation (CID) of $Cr(CO)_x^+$ species results in the sequential elimination of CO molecules. This is apparent in the data for $Cr(CO)_6^+$, shown in Figure 1, which is typical of all the chromium carbonyl cations. No product ions with different numbers of carbon and oxygen atoms are observed. This observation is easily rationalized because an individual CO bond is substantially stronger than even the sum of the metal carbonyl bonds in $Cr(CO)_6^+$. Other than CID, the only other process observed is the ligand exchange reaction 5. Ligand

$$CrCO^+ + Xe \rightarrow CrXe^+ + CO \qquad (5)$$

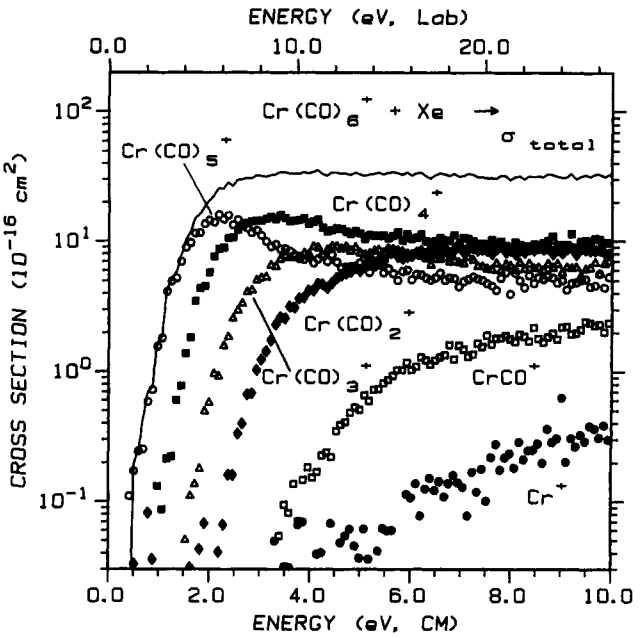

Figure 1. Cross sections for reaction of $Cr(CO)_6^+$ with Xe at 0.25 mTorr as a function of relative kinetic energy (lower axis) and laboratory energy (upper axis). Sequential loss of CO ligands occurs to form $Cr(CO)_5^+$ (open circles), $Cr(CO)_4^+$ (solid squares), $Cr(CO)_3^+$ (open triangles), $Cr(CO)_2^+$ (solid diamonds), $CrCO^+$ (open squares), and Cr^+ (solid circles). The solid line represents the total cross section.

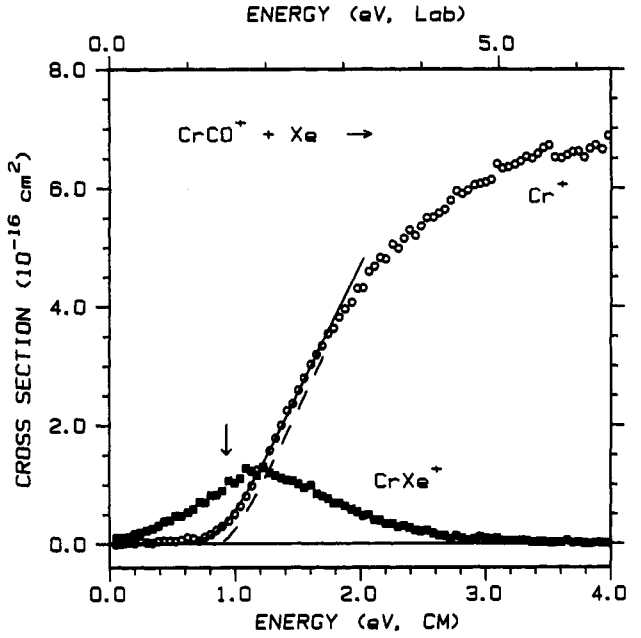

Figure 2. Cross sections for reaction of $CrCO^+$ with Xe at 0.05 mTorr to form Cr^+ (open circles) and $CrXe^+$ (solid squares) as a function of relative kinetic energy (lower axis) and laboratory energy (upper axis). The dashed line is the model of eq 4 with the parameters in Table IV for 0 K reactants. The solid line is this model convoluted over the translational, vibrational, and rotational energy distributions of the reactants. The vertical arrow indicates the 0 K threshold for loss of a CO ligand at 0.93 eV.

exchange is presumably taking place with $Cr(CO)_x^+$, $x \geq 2$, as well; however, we did not look for these products explicitly for $x = 2$ and 3, while those for $x = 4$–6 have masses larger than the detection limit ($\sim$240 m/z) of our detector quadrupole mass filter.

Results for the interaction of $CrCO^+$ with Xe are shown in Figure 2. The major product is Cr^+, which has a cross section with an apparent threshold of $\sim$0.8 eV. Ligand exchange to form $CrXe^+$ has a lower apparent threshold and a cross section

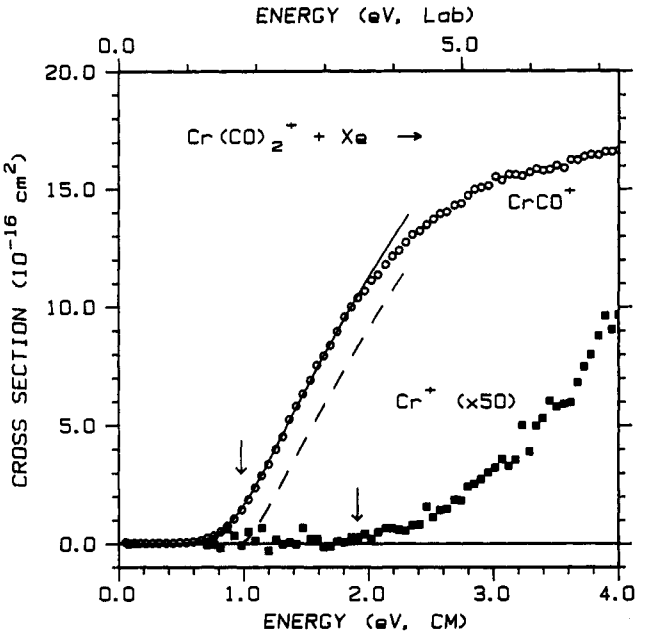

Figure 3. Cross sections for reaction of $Cr(CO)_2^+$ with Xe at 0.05 mTorr to form $CrCO^+$ (open circles) and Cr^+ (solid squares, increased by a factor of 50) as a function of relative kinetic energy (lower axis) and laboratory energy (upper axis). The dashed line is the model of eq 4 with the parameters in Table IV for 0 K reactants. The solid line is this model convoluted over the translational, vibrational, and rotational energy distributions of the reactants. Vertical arrows indicate the 0 K thresholds for loss of one CO at 0.98 eV and two CO ligands at 1.91 eV.

that peaks near the CID threshold. This behavior is clearly due to competition between the ligand exchange process and the favored CID reaction. The mass resolution of the quadrupole mass spectrometer was sufficiently low that the cross section shown in Figure 2 for $CrXe^+$ should represent the product intensities for all isotopes of Xe.

Results for CID of $Cr(CO)_2^+$ with Xe are shown in Figure 3. The major product, $CrCO^+$, has an apparent threshold similar to that for Cr^+ in Figure 2 and a magnitude about twice as large. Loss of two CO ligands to form Cr^+ is quite inefficient and has a cross section that rises very slowly from a higher apparent threshold. As shown in Figure 4, CO loss from $Cr(CO)_3^+$ has a much lower apparent threshold and a much larger cross section than in the $Cr(CO)_2^+$ and $CrCO^+$ systems. This $Cr(CO)_2^+$ cross section reaches a maximum at the apparent threshold for $CrCO^+$ formation, showing that the CO molecules are lost sequentially. Formation of Cr^+ again has a small cross section that rises slowly from threshold.

The CID pattern in $Cr(CO)_4^+$, shown in Figure 5, is similar to that of $Cr(CO)_3^+$ in that the apparent threshold for the loss of a single CO is fairly low, <0.2 eV. The cross section for $Cr(CO)_3^+$ rises to a sharp maximum at the threshold for a second CO loss and declines at higher energies, again indicating sequential CO loss. The CID pattern for $Cr(CO)_5^+$, shown in Figure 6, is similar to that of $Cr(CO)_4^+$ and $Cr(CO)_3^+$. The threshold for the loss of a single CO is again <0.2 eV. In contrast, the apparent threshold for loss of the first CO from $Cr(CO)_6^+$, Figure 7, is about 1 eV, much higher than those for $Cr(CO)_3^+$, $Cr(CO)_4^+$ and $Cr(CO)_5^+$.

$(CO)_xCr^+$–CO BDEs from Primary Thresholds. Our best measure of the bond dissociation energies for the chromium carbonyl ions comes from analyses of the primary dissociation channels, reactions 6, where $x = 1$–6. Listed in Table IV are the

$$Cr(CO)_x^+ + Xe \rightarrow Cr(CO)_{x-1}^+ + CO + Xe \qquad (6)$$

optimized parameters of eq 4 obtained from an analysis of reactions 6 for between two and six independent data sets for all

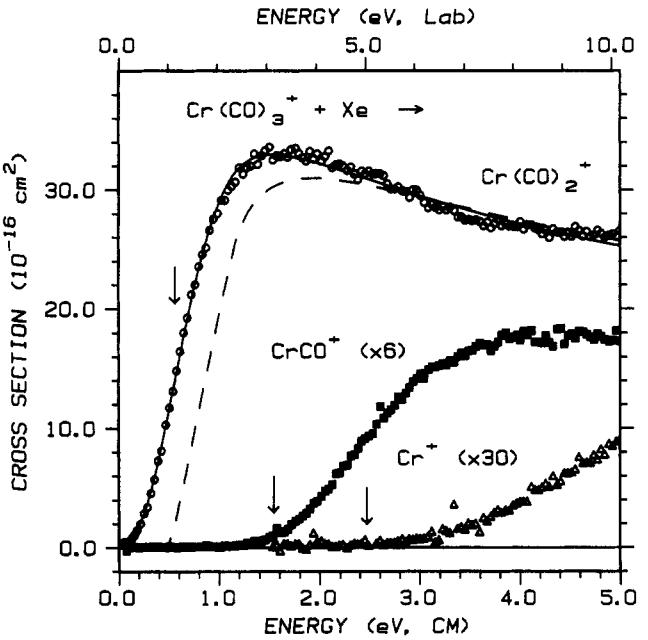

Figure 4. Cross sections for reaction of $Cr(CO)_3^+$ with Xe to form $Cr(CO)_2^+$ (open circles, data extrapolated to zero Xe pressure), $CrCO^+$ (solid squares, increased by a factor of 6, 0.05 mTorr of Xe), and Cr^+ (open triangles, increased by a factor of 30, 0.05 mTorr of Xe) as a function of relative kinetic energy (lower axis) and laboratory energy (upper axis). The dashed line is the model of eq 4 with the parameters in Table IV for 0 K reactants. The solid line is this model convoluted over the translational, vibrational, and rotational energy distributions of the reactants. Vertical arrows indicate the 0 K thresholds for loss of one, two and three CO ligands at 0.56, 1.54, and 2.47 eV, respectively.

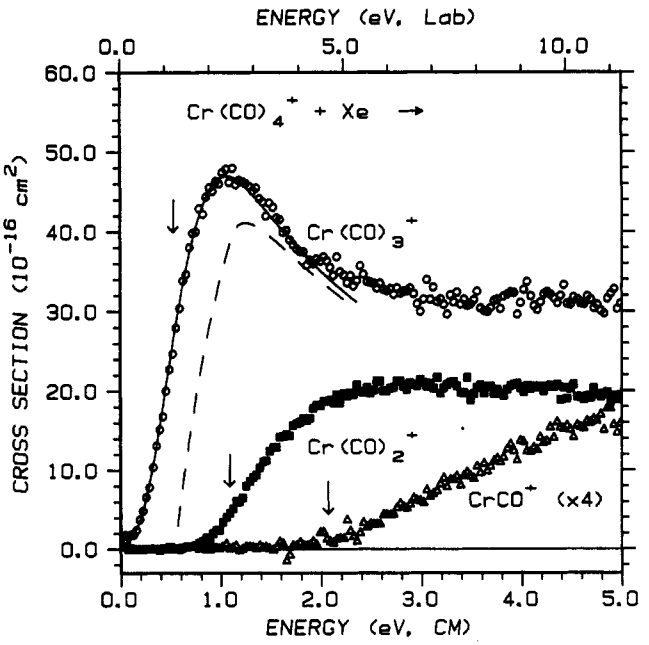

Figure 5. Cross sections for reaction of $Cr(CO)_4^+$ with Xe at 0.3 mTorr to form $Cr(CO)_3^+$ (open circles), $Cr(CO)_2^+$ (solid squares), and $CrCO^+$ (open triangles, increased by a factor of 4) as a function of relative kinetic energy (lower axis) and laboratory energy (upper axis). The dashed line is the model of eq 4 with the parameters in Table IV for 0 K reactants. The solid line is this model convoluted over the translational, vibrational, and rotational energy distributions of the reactants. Vertical arrows indicate the 0 K thresholds for loss of one, two, and three CO ligands at 0.53, 1.09, and 2.07 eV, respectively.

ions. Because the vibrational, rotational, and translational energy distributions of the ions are explicitly included in our modeling, these thresholds correspond to 0 K values. In the cases of $Cr(CO)_6^+$ and $Cr(CO)_5^+$, two analyses are listed in Table IV: one including the RRKM analysis of the lifetime of the dissociating

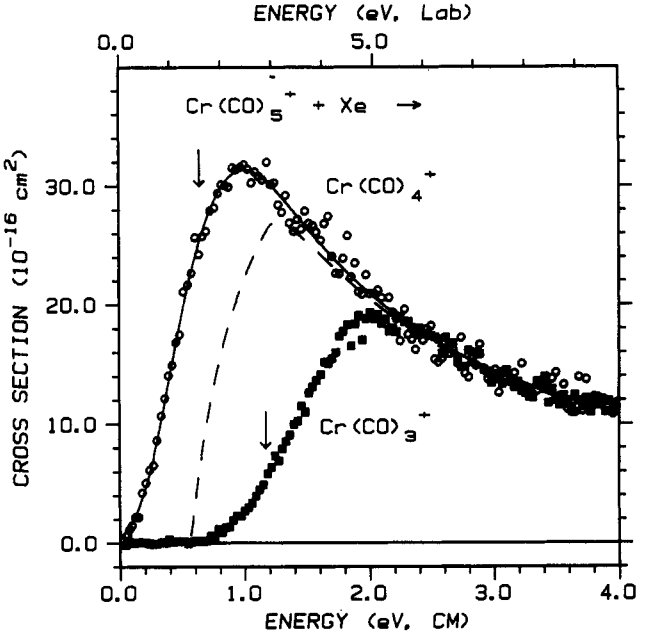

Figure 6. Cross sections for reaction of $Cr(CO)_5^+$ with Xe at 0.05 mTorr to form $Cr(CO)_4^+$ (open circles) and $Cr(CO)_3^+$ (solid squares) as a function of relative kinetic energy (lower axis) and laboratory energy (upper axis). The dashed line is the model of eq A7 with the parameters in Table IV for 0 K reactants. The solid line is this model convoluted over the translational, vibrational, and rotational energy distributions of the reactants. Vertical arrows indicate the 0 K thresholds for loss of one and two CO ligands at 0.64 and 1.17 eV, respectively.

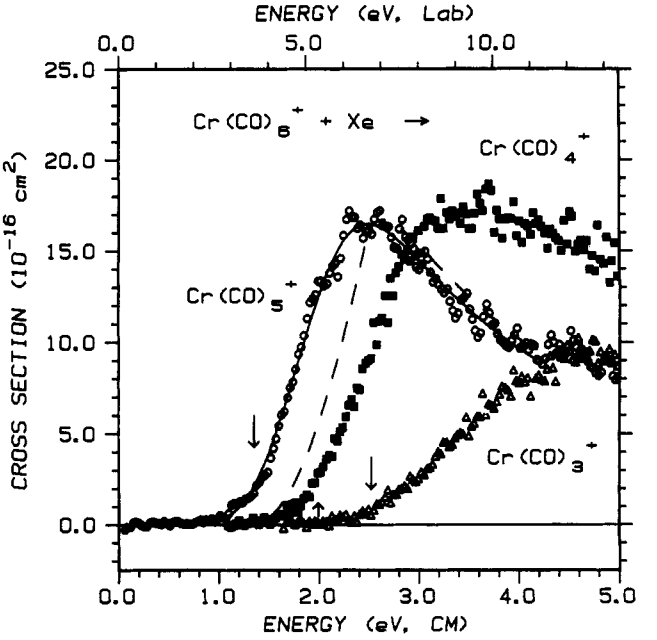

Figure 7. Cross sections for reaction of $Cr(CO)_6^+$ with Xe to form $Cr(CO)_5^+$ (open circles, data extrapolated to zero Xe pressure), $Cr(CO)_4^+$ (solid squares, 0.05 mTorr of Xe), and $Cr(CO)_3^+$ (open triangles, 0.05 mTorr of Xe) as a function of relative kinetic energy (lower axis) and laboratory energy (upper axis). The dashed line is the model of eq A7 with the parameters in Table IV for 0 K reactants. The solid line is this model convoluted over the translational, vibrational, and rotational energy distributions of the reactants. Vertical arrows indicate the 0 K thresholds for loss of one, two, and three CO ligands at 1.35, 1.99, and 2.52 eV, respectively.

ion and one ignoring this effect. As the data in Table IV shows, this lifetime effect is substantial for the dissociation of $Cr(CO)_6^+$ and is considerably smaller for $Cr(CO)_5^+$. We verified that the dissociation of $Cr(CO)_4^+$ ion is sufficiently prompt that a negligible kinetic shift results. Lifetime effects for the species $Cr(CO)_3^+$, $Cr(CO)_2^+$, and $CrCO^+$ should also be negligible.

TABLE IV: Summary of Parameters of Eq 4 for Modeling Primary CO Loss[a]

species	E_0 (eV)	σ_0	n
Cr^+–CO	0.93(0.04)	6.6(1.1)	1.5(0.1)
$(CO)Cr^+$–CO	0.98(0.03)	20(3)	1.5(0.1)
$(CO)_2Cr^+$–CO	0.56(0.06)	50(8)	1.2(0.2)
$(CO)_3Cr^+$–CO	0.53(0.08)	72(12)	1.2(0.2)
$(CO)_4Cr^+$–CO	0.67(0.04)	54(8)	0.9(0.1)
	0.64(0.03)[b]	53(8)[b]	0.8(0.1)[b]
$(CO)_5Cr^+$–CO	1.58(0.12)	42(8)	2.0(0.5)
	1.35(0.08)[b]	39(10)[b]	1.9(0.5)[b]

[a] Uncertainties in parenteses. [b] Values obtained when using the RRKM analysis, eq A7, see text.

We take the 0 K thresholds to equal $D[(CO)_{x-1}Cr^+–CO]$, implicitly assuming that there are no activation barriers to dissociation in excess of the endothermicity. Theoretical considerations show that this is a good assumption for metal carbonyl species,[34] and we have shown in the $Fe(CO)_5^+$ system that this assumption leads to accurate BDEs.[3] In the present system, this assumption is further validated by the agreement between the sum of the $Cr(CO)_x^+$ BDEs and $\Delta_rH°(1)$, a point addressed in detail below. We believe that this assumption holds because CID involves energy transfer and dissociation processes that occur slowly (especially at threshold, see discussion above). It is inappropriate to consider such reactions as sudden or as vertical transitions, such as those inherent in many photochemical processes. Even the presence of different product isomers should not affect the accuracy of the measured thresholds because the highly energized reactant should be capable of exploring the various dissociation possibilities thereby forming the lowest energy isomer *at threshold*. Exceptions might occur, however, when different isomers are associated with different electronic states or spins, a potential complication addressed in more detail below.

$(CO)_{x-1}Cr^+$–CO BDEs from Secondary Thresholds. In principle, the difference in the thermodynamic thresholds for loss of successive CO ligands should yield thermochemical information. For example, the difference between the thresholds of processes 7 and 6 gives the BDE for $(CO)_{x-2}Cr^+$–CO.

$$Cr(CO)_x^+ + Xe \rightarrow Cr(CO)_{x-2}^+ + 2CO + Xe \qquad (7)$$

Indeed, such secondary threshold analysis has been used to obtain successive BDEs for $M(H_2O)_n^+$ and $Mn_2(CO)_n^+$ systems.[35,36] The advantages of this approach are that large systematic errors are avoided and an absolute energy scale is not required. The difficulty with extracting accurate thermodynamic information from secondary thresholds is that the probability for dissociation at the true thermodynamic threshold decreases as the extent of dissociation increases because the neutral products in the primary dissociation events can carry away energy. In addition, we have found that the multiple collision problem discussed above is enhanced for secondary dissociations because the energy added by the additional collision can induce much more efficient dissociation for these improbable events near threshold. Notice that the first effect acts to increase the apparent threshold, while the latter effect tends to decrease it, such that they can fortuitously cancel to a large extent.

BDEs obtained from an analysis of secondary thresholds from various reactant species $Cr(CO)_x^+$ without consideration of lifetime effects are listed in Table V along with the thermodynamic thresholds calculated from the primary threshold energies in Table IV. For loss of two carbonyl ligands from $Cr(CO)_2^+$, $Cr(CO)_3^+$, and $Cr(CO)_5^+$, the measured thresholds are within experimental error of the thermodynamic ones. Kinetic shifts and pressure effects are small. This agreement helps confirm the accuracy of the bond energies determined from the primary thresholds. For $Cr(CO)_6^+$ (where a strong pressure effect was observed on the primary CO loss channel) and $Cr(CO)_4^+$, decreasing threshold energies with increasing pressure are found for loss of two and three carbonyl ligands. Analyses of these data extrapolated to zero Xe pressure yield thresholds that lie somewhat above the thermodynamic thresholds, consistent with small kinetic shifts. Overall, the larger uncertainties associated with the secondary thresholds lead us to recommend primary CID thresholds as the most accurate source of thermochemical information, as also concluded in our CID study of $Fe(CO)_x^+$.[3]

TABLE V: Summary of Values for Thresholds (eV) for Loss of Multiple CO Ligands[a]

process	thermodynamic[b]	high pressure	low pressure	zero pressure
$Cr(CO)_2^+ \rightarrow Cr^+$	1.91(0.05)	1.94(0.08)	2.03(0.10)	
$Cr(CO)_3^+ \rightarrow CrCO^+$	1.54(0.07)	1.55(0.11)	1.53(0.05)	1.60(0.05)
$Cr(CO)_4^+ \rightarrow Cr(CO_2)^+$	1.09(0.10)	1.11(0.09)	1.25(0.11)	1.42(0.12)
$Cr(CO)_5^+ \rightarrow Cr(CO)_3^+$	1.20(0.09)	1.25(0.04)	1.26(0.04)	1.25(0.04)
	1.17(0.09)			
$Cr(CO)_6^+ \rightarrow Cr(CO)_4^+$	2.25(0.13)	2.00(0.03)	2.11(0.06)	2.52(0.03)
	1.99(0.09)			
$Cr(CO)_6^+ \rightarrow Cr(CO)_3^+$	2.78(0.15)	2.48(0.03)	2.89(0.04)	3.23(0.05)
	2.52(0.12)			

[a] Uncertainties in parentheses. High and low pressures refer to experiments performed at Xe neutral gas pressures of ~0.30–0.25 and ~0.05 mTorr, respectively. Zero pressure refers to data extrapolated as discussed in the text. [b] Thresholds calculated from primary threshold energies listed in Table IV. The second values are obtained by using the RRKM analysis.

Cr^+–Xe BDE. Analysis of the threshold for the ligand exchange reaction 5 yields a threshold of 0.23 ± 0.08 eV. Because this energy is the difference between the binding energies of CO and Xe to Cr^+, $D(Cr^+–Xe)$ is determined as 0.7 ± 0.1 eV given the Cr^+–CO bond energy of 0.93 ± 0.04 eV (Table IV). This value lies between those we have previously measured for V^+–Xe (0.84 ± 0.17 eV)[37] and Fe^+–Xe (0.39 ± 0.09 eV).[3] One means of rationalizing these relative M^+–Xe BDEs is to consider the ground-state electronic configurations of the atomic metal ions.[38] $D(Cr^+–Xe)$ is weaker than $D(V^+–Xe)$ because $Cr^+(^6S,3d^5)$ is forced to place an electron in the $3d\sigma$ orbital while $V^+(^5D,3d^4)$ can leave this orbital empty. $D(Fe^+–Xe)$ is weaker still because Fe^+-$(^6D,4s^13d^6)$ occupies the 4s orbital, increasing the metal–ligand repulsion.

It is also interesting to compare the Cr^+–Xe BDE to that for Cr^+–Ar, measured to be 0.29 ± 0.04 eV[39] and calculated to be 0.23 eV.[40] We recently noted that M^+–Ar and M^+–Xe BDEs for M = Fe and Co increase from a zero intercept almost linearly with increasing polarizability of the rare gas ligand.[41] Based on the polarizabilities of Xe (4.02 Å^3) and Ar (1.64 Å^3),[42] an M^+–Xe bond should be ~2.45 times stronger than an M^+–Ar bond, consistent with the relative values of $D(Cr^+–Xe)$ measured here and the literature values for $D(Cr^+–Ar)$. A similar comparison can be found for VAr^+ and VXe^+ BDEs.[43,44] More detailed accounts of the bonding between transition metal ions and rare gases are contained in recent review articles.[45]

Discussion

Comparison with Literature Thermochemistry. As pointed out earlier, a test for the accuracy of the sequential BDEs of $Cr(CO)_x^+$ is agreement between the sum of the BDEs and $\Delta_rH°(1)$. Our 0 K BDEs listed in Table IV are converted to 298 K values as discussed above and listed in Table I. In our CID experiments, the sum of the six 298 K BDEs is 5.43 ± 0.17 eV if lifetime effects are not included and 5.17 ± 0.14 eV is lifetime effects are included in the analysis. Both totals are in reasonable agreement with $\Delta_rH_{298}°(1)$, 5.23 ± 0.09 eV. This agreement contrasts with previous studies, Table I, where the sums of the bond energies exceed $\Delta_rH_{298}°(1)$ by considerable amounts. Because the bond energy sums in these studies come from the difference in the appearance energies (AEs) of Cr^+ and $Cr(CO)_6^+$, the most likely explanation for these discrepancies is that the measured AEs for Cr^+ are too high due to kinetic shifts. This is because the loss

of all six CO ligands from ionized $Cr(CO)_6^+$ is improbable at its threshold, such that the true thermodynamic threshold is difficult to observe.

Previously, the closest agreement with the literature was obtained in the photoionization study of Meisels and co-workers.[16] These authors assumed that their appearance energies (AEs) constituted 298 K thermochemistry and compared their results to the literature by calculating an average value for the Cr–CO bond in $Cr(CO)_6$. They obtained 28.3 ± 0.4 kcal/mol based on their value for the appearance energy of Cr^+, $AE(Cr^+) = 14.13 \pm 0.11$ eV, and an IE for Cr of 6.674 eV taken from the 59th edition of the *CRC Handbook of Chemistry and Physics*. This average energy compared well with the 27.1 kcal/mol value cited by Cotton et al.[46] (although the average BDE that we calculate from the heat of formation obtained by Cotton et al.[18] is 29.5 kcal/mol) and the small difference was attributed to kinetic shifts. As noted above, however, the heat of formation for $Cr(CO)_6$ of Cotton et al. is now believed to be inaccurate by 23.4 kcal/mol[21] and IE(Cr) = 6.766 69 ± 0.000 04 eV.[47] Based on the thermochemistry in Table II, the correct value for the average Cr–CO bond in $Cr(CO)_6$ is 25.6 ± 0.2 kcal/mol at 298 K, well below the value obtained by Meisels and co-workers, and well outside of experimental error.

Rather than compare the absolute BDEs in Table I, it is more useful to compare the *trends* in these BDEs. As noted in the Introduction, the mass spectrum of $Cr(CO)_6$ at elevated ionization energies has large abundances of $Cr(CO)_6^+$, $Cr(CO)_2^+$, and $Cr(CO)^+$ and small abundances of $Cr(CO)_5^+$, $Cr(CO)_4^+$, and $Cr(CO)_3^+$. The relatively strong BDEs of the former three ions and the weak BDEs of the latter three ions (Table I) easily explains this observation. In this respect, the BDEs from previous studies and those observed here are in *qualitative* agreement with one another (Table I). We note that our results for $D[(CO)_5Cr^+–CO]$ are consistent with those of Michels et al.[15] and Meisels and co-workers,[16] which is reasonable because $AE[Cr(CO)_5^+]$ should be influenced the least by kinetic shifts. Their BDEs for $Cr(CO)_5^+$, $Cr(CO)_4^+$, and $Cr(CO)_3^+$ are the weakest measured, and their BDEs for Cr^+–CO and $(CO)Cr^+$–CO are comparable to one another, as we also observe. Finally, we note that our values for $D(Cr^+–CO)$ and $D[(CO)Cr^+–CO]$ are in fairly good agreement with the ab initio theoretical values of 0.90 and 0.93 eV, respectively, corrected to 298 K from the D_es calculated by Barnes et al.[9] The agreement is comparable to that observed between our experimental and their theoretical results for $FeCO^+$ and $Fe(CO)_2^+$ BDEs.[3] This agreement tends to confirm the theoretical picture that the bonding in the cationic metal mono- and dicarbonyls is largely electrostatic with minor contributions from backbonding.

It is necessary to consider whether the BDEs for $Cr(CO)_5^+$ and $Cr(CO)_6^+$ obtained with and without lifetime considerations are more accurate. Our prejudice is to include the lifetime effect because this consideration has proved to be critical in the accurate evaluation of the BDEs for transition metal cluster ions.[48-50] Nevertheless, it is desirable to consider this question independently. Comparison of the sum of the BDEs with $\Delta_r H_{298}°(1)$ also suggests that the lifetime effect should be included, although this cannot be used as a definitive criterion to choose because the literature value for $\Delta_r H_{298}°(1)$ is within experimental error of both sums. Comparison between the present values and those obtained in previous studies might be useful (indeed the BDEs for $Cr(CO)_5^+$ and $Cr(CO)_6^+$ obtained by Michels et al.[15] are in good agreement with our values obtained including the lifetime effects), but in none of these previous studies were the internal energies or the lifetimes of the ions explicitly considered. Because these two effects operate on the apparent thresholds in opposite directions, such comparisons are probably not quantitatively useful.

One comparison that may be useful is the observation made by Lloyd and Schlag[26] that a second rise in their ionization cross section can probably be assigned to the onset for $Cr(CO)_5^+$ formation, although this assignment is not definitive because this ion is not actually observed in their work. If correct, the onset for this "second rise" yields an *upper* limit to the $(CO)_5Cr^+–CO$ BDE of 1.12 ± 0.04 eV, although it seems probable that this onset could be too low due to contributions from the internal energy in the room temperature $Cr(CO)_6$. If we correct this onset for the average vibrational energy of the parent molecule, 0.32 eV, then the upper limit becomes 1.44 eV, clearly suggesting that our lower BDE is correct. Overall, the evidence seems to suggest that our best chromium carbonyl ion BDEs are those determined by including the lifetime effect.

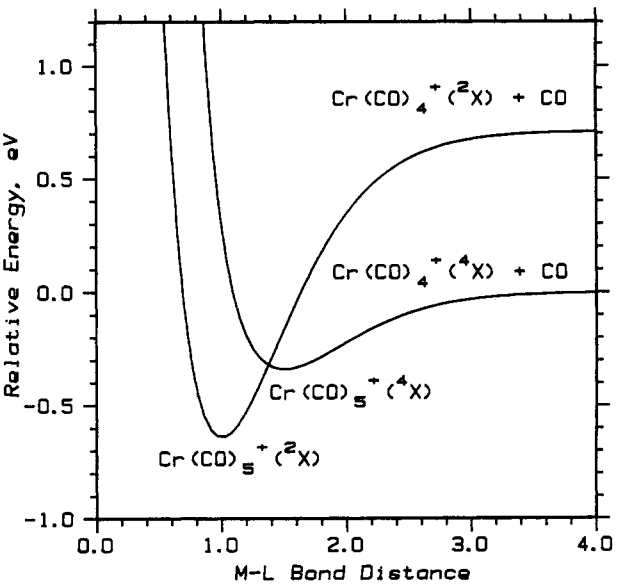

Figure 8. Qualitative potential energy surfaces for dissociation of $Cr(CO)_5^+$ illustrating how electronic states can influence bond dissociation energies.

Trends in Sequential Bond Energies. The nonmonotonic variation in chromium carbonyl cation BDEs with decreasing ligation cannot be rationalized on the basis of decreasing steric effects or increasing effective charge at the metal center. Instead, we turn to a consideration of the electronic structure of these species in order to explain the trends in the sequential bond energies. In our recent study of the CID of $Fe(CO)_x^+$ ions,[3] we explained similar nonmonotonic variations in the sequential BDEs in terms of changes in spin (or lack thereof) of the metal carbonyl fragments that accompany the removal of CO molecules. The possible effects of spin conservation have also been used to explain the observed rates of decomposition and recombination reactions of $Mn(CO)_x^+$,[4] $Cr(CO)_x$,[51,52] and $Fe(CO)_x$.[53] For the chromium carbonyl cation system, the ground electronic state of Cr^+ is $^6S(3d^5)$[38] and the ground electronic states of $CrCO^+$ and $Cr(CO)_2^+$ have been calculated to be $^6\Sigma^+$ and $^6\Sigma_g^+$, respectively.[9] $Cr(CO)_6^+$, formed by removing an electron from singlet $Cr(CO)_6$, is likely to be a doublet in its ground electronic state. Thus, as successive CO molecules are added to $Cr(CO)_2^+$, the spin of the ground states of the chromium carbonyl cations must change.

Empirically, we find that the BDEs of $CrCO^+$ and $Cr(CO)_2^+$ are relatively strong. Because these species and Cr^+ all have sextet ground states, this suggests that strong BDEs are associated with dissociations that are spin allowed, a conclusion also reached in our study of $Fe(CO)_x^+$.[3] On this basis, the strong $(CO)_5Cr^+–CO$ BDE suggests that $Cr(CO)_5^+$ has a doublet ground state. A weak $(CO)_4Cr^+–CO$ BDE can be rationalized by the following arguments and the qualitative potential energy surfaces shown in Figure 8. Dissociation of $Cr(CO)_5^+$ along the diabatic (spin-allowed doublet) surface would yield a dissociation threshold similar to that of $Cr(CO)_6^+$, whose dissociation is believed to be spin-allowed. If the ground state of $Cr(CO)_4^+$ is a quartet,

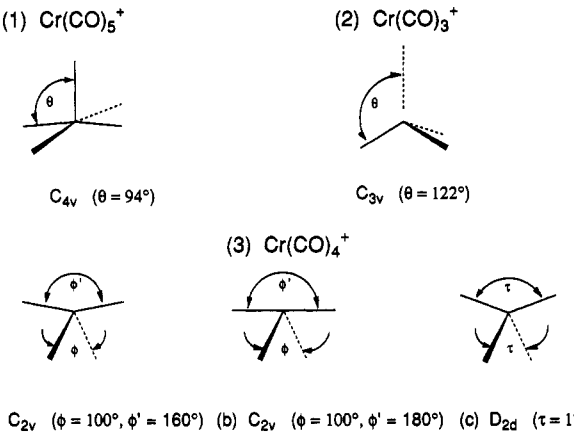

Figure 9. Geometries for $Cr(CO)_5^+$ (1), $Cr(CO)_3^+$ (2), and $Cr(CO)_4^+$ (3), based on calculations by Elian and Hoffmann, ref 54.

however, then dissociation along the *adiabatic* surface (i.e., crossing from the doublet to the quartet surface) will lead to a much lower dissociation threshold and hence $D[(CO)_4Cr^+–CO]$ will be lower than $D[(CO)_5Cr^+–CO]$.

To understand the bond energy patterns more completely, it would be desirable to know the ground electronic states of $Cr(CO)_5^+$, $Cr(CO)_4^+$, and $Cr(CO)_3^+$. Because no calculations have been performed specifically on these species, we turn to the extended Huckel calculations carried out on $M(CO)_x$ systems by Elian and Hoffmann.[54] This work computes the energies of metal d orbitals as the number of d electrons and the geometry of $M(CO)_x$ are varied. For a d^5 system (such as Cr^+), the optimum geometries expected for $Cr(CO)_5^+$, $Cr(CO)_4^+$, and $Cr(CO)_3^+$ are shown in Figure 9. We also consider a planar $Cr(CO)_3^+$ molecule, $\theta = 90°$, because Burdett[55] finds that the geometry of this species is sensitive to the spin state and Elian and Hoffmann note that the surface is quite flat. In order to predict the ground states of these species, we also need to know the exchange energy lost upon pairing electrons. We take the sextet–quartet and quartet–doublet spin pairing energies to be 2.4 eV (the difference in energy between the ^4D and ^6S states of Cr^+) and 1.3 eV (the difference in energy between the ^2I and ^4D states of Cr^+), respectively.[38] We use these energies because similar values of 2.5 and 1.1 eV are obtained from theoretically calculated values for the exchange energy lost upon pairing the d electrons of Cr^+.[56] Values that are about 30% higher are obtained from formulae given by Griffith[57] for an octahedral ligand field with Racah parameters for Cr^+ taken from Catalan et al.[58]

Combining these spin pairing energies with the orbital energies allows a prediction of the relative energies of the different spin states for $Cr(CO)_5^+$, $Cr(CO)_4^+$, and $Cr(CO)_3^+$. For $Cr(CO)_5^+$, we find that the ground state should be a doublet with a quartet state about 0.9 eV higher in energy. Any sextet state is predicted to lie over 3.6 eV higher than the doublet. This is in agreement with the assignment made above on the basis of the large BDE for $Cr(CO)_6^+$. The ground electronic state of $Cr(CO)_3^+$ (θ = 122°) is also predicted to be a doublet with a quartet and sextet state approximately 1.5–1.8 eV higher in energy. In this case, the large change in BDE noted between $Cr(CO)_2^+$ and $Cr(CO)_3^+$ could be explained by the process $Cr(CO)_3^+(^2X) \rightarrow Cr(CO)_2^+(^6X) + CO(^1\Sigma^+)$, although it is interesting that the spin change is sextet–doublet rather than a sextet–quartet as might have been guessed. However, if $Cr(CO)_3^+$ is planar ($\theta = 90°$), then the ground state is sextet, with a quartet and doublet state approximately 1.3–1.6 eV higher in energy. Now, the change in BDE cannot be an electronic effect because both $Cr(CO)_3^+$ and $Cr(CO)_2^+$ are ground-state sextets. In this case, we attribute the drop in BDE to increased ligand–ligand repulsions, an idea that can be verified by comparison with our recent results for $Ni(CO)_x^+$ ions,[59] which all have doublet spin ground states (due to the d^9 configuration). There we measured that $D[(CO)_2Ni^+–CO]$ was 53 ± 6% of $D[(CO)Ni^+–CO]$, very similar to the ratio obtained here, $D[(CO)_2Cr^+–CO] = 57 \pm 8\%$ of $D[(CO)Cr^+–CO]$.

An unambiguous prediction of the ground state of $Cr(CO)_4^+$ is not easily made based on the extended Huckel calculations, which indicate that there are low-lying doublet, quartet and sextet states comparable in energy.[60] The low $(CO)_3Cr^+–CO$ BDE may imply that the $Cr(CO)_4^+$ species has a quartet ground state, thus making the adiabatic dissociation pathways, $Cr(CO)_5^+(^2X) \rightarrow Cr(CO)_4^+(^4X) + CO(^1\Sigma^+)$ and $Cr(CO)_4^+(^4X) \rightarrow Cr(CO)_3^+(^6X \text{ or } ^2X) + CO(^1\Sigma^+)$, both spin-forbidden. It is also possible that $Cr(CO)_4^+$ has a sextet ground state, because the relative BDEs of $Cr(CO)_3^+$ and $Cr(CO)_4^+$ are comparable with those of $Ni(CO)_3^+$ and $Ni(CO)_4^+$.[59] This still implies a spin-forbidden adiabatic dissociation pathway for $Cr(CO)_5^+(^2X)$.

Conclusions

We report the first systematic measurement of the sequential $Cr(CO)_6^+$ BDEs by collision-induced dissociation, a method that avoids possible kinetic shift problems inherent in photon- and electron-induced ionization and dissociation measurements. We find good agreement between the sum of the six sequential BDEs and the literature value for $\Delta_rH°(1)$, which demonstrates that internal energies must be included in CID threshold evaluations. We estimate lifetime effects to be appreciable in the dissociation of the largest ion studied, $Cr(CO)_6^+$, nonnegligible for $Cr(CO)_5^+$, and absent for the smaller chromium carbonyl ions.

We interpret nonmonotonic changes in sequential BDEs in terms of spin changes induced by the increasing ligand field. Our results suggest that $Cr(CO)_6^+$ and $Cr(CO)_5^+$ have doublet ground states, and more speculatively, that $Cr(CO)_3^+$ and $Cr(CO)_4^+$ have doublet and quartet ground states, respectively, or alternatively, that have sextet ground states. The BDE for $CrXe^+$ is also reported.

Acknowledgment. This work is supported by the National Science Foundation, Grant No. CHE-9221241. F.A.K. thanks Prof. Tom Richmond for several enlightening conversations.

Appendix: Statistical Modelling of Collision-Induced Dissociation Thresholds

In previous work,[48] we have outlined a method of analyzing the threshold behavior of CID cross sections that incorporates an energy-dependent unimolecular rate constant for dissociation. This is needed to account for the effects of a finite experimental time window τ available to dissociating ions. In this appendix, we modify this method to incorporate the distribution of internal energies available to the ion prior to the collision. The derivation of this model demands that it revert to the empirical form of eq 4 in the limit that the dissociation lifetime is fast. This requirement ensures that the model that has proven so useful in analyzing numerous CID reactions is retained.[3,41,48-50,61] Further, we correct a conceptual error in the previous derivation and evaluate the consequences of this error on past results.

The unimolecular rate constant is given by RRKM theory[62] as

$$k(E_T - E_0) = s\frac{Q^\dagger N^\dagger(E_T - E_0)}{Qh\rho(E_T)} \qquad \text{(A1)}$$

where $N^\dagger(E_T - E_0)$ is the sum of states of the transition state at an energy $(E_T - E_0)$ above the dissociation energy, and $\rho(E_T)$ is the reactant density of states at the total energy E_T. $Q^\dagger$ and Q are the rotational partition functions of the transition state and the energized cluster, respectively. For dissociation of a species like $Cr(CO)_x^+$, the reaction path degeneracy s is equal to x. The expressions for the sum and density of states as a function of the

ion internal energy are evaluated by using the Beyer–Swinehart algorithm[32] to directly count states.

The ratio of the rotational partition functions, $Q^\dagger/Q$, is evaluated following the method of Waage and Rabinovitch.[63] They show that within a rigid-rotor approximation $Q^\dagger/Q = \langle\langle r_m^2\rangle\rangle/r_e^2$, where r_e is the equilibrium distance between the dissociating fragments and $\langle\langle r_m^2\rangle\rangle$ is the apparent square of the distance between the centers of masses of the dissociating fragments at the transition state. For an ion–molecule potential, $V(r) = -\alpha e^2/2r^4$ where α is the polarizability of the neutral fragment and e is the charge on the electron, the formulae of Waage and Rabinovitch can be used to show that $\langle\langle r_m^2\rangle\rangle = (\pi\alpha e^2/2kT)^{1/2}$. For chromium carbonyls, the result is $\langle\langle r_m^2\rangle\rangle = 41$ Å^2, independent of which $Cr(CO)_x^+$ species is considered. Combined with $r_e = 2.6$ Å,[64] assumed to be approximately the same for $Cr(CO)_5^+$ as for $Cr(CO)_6^+$ (the only two species where the RRKM calculations are needed), $Q^\dagger/Q \approx 6$. The use of this ratio rather than unity increases the bond energies obtained for $Cr(CO)_6^+$ by 0.03 eV and those for $Cr(CO)_5^+$ by 0.01 eV.

The empirical threshold model describing the translational energy (E) dependence of the CID cross section, given by eq 4 in the text, can be derived from the relationship given in eq A2,

$$\sigma(E) = \int_0^{b_{max}} 2\pi\Omega(E) b\, db \qquad (A2)$$

where $\Omega(E)$ is the opacity function or probability of reaction and b is the impact parameter. In its simplest form, the line-of-centers (LOC) model,[65] the relative reactant energies must be nonzero after surmounting the thermodynamic (E_0) and centrifugal $E(b/d)^2$ barriers for reaction to occur, where d is the distance of closest approach between the reactants. As a result, b must satisfy the relation, $E - E_0 - E(b/d)^2 \geq 0$. If we assume that internal energy of the ion is also available to overcome the effective barrier, then after rearrangement, this relationship becomes

$$b^2 \leq d^2(E_T - E_0)/E \qquad (A3)$$

where E_T is the sum of the relative translational, rotational, and vibrational energies, $E + E_{rot} + \sum g_i E_i$. If b_{max} is defined as the largest impact parameter for reaction, then $b_{max}^2 = d^2(E_T - E_0)/E$. If $\Omega(E)$ is set equal to unity, then eq A2 becomes $\sigma(E) = \pi d^2(E_T - E_0)/E$, the LOC model, equivalent to eq 4 with $n = 1$ and $\sigma_0 = \pi d^2$. The more general model of eq 4 assumes that b^2 has a similar form to eq A3, but arbitrarily introduces the parameter n so that $b_{max}^2 = d^2(E_T - E_0)^n/E$. This can be justified in several ways as we have done elsewhere.[61,66,67]

In our previous work, we extended the relationship in eq A3 to the CID process by noting that collisions between the ion and the rare gas atom will deposit only a portion of the relative collision energy into internal energy of the ion. Thus, we *assumed* that b^2 could take a similar form to that above,

$$b^2 = d^2(E_T - \Delta E - E_0)^n/E \qquad (A4)$$

where ΔE is defined as the energy that remains in relative translational motion after the collision between the reactants, and thus, $E - \Delta E$ is the energy that is actually transferred into the internal energy of the dissociating ion by this collision at a relative translational energy E. The interdependence of b and ΔE was rationalized on the basis that grazing collisions at large values of b can only result in small values of $E - \Delta E$, while small impact parameters lead to the largest amounts of energy deposited. Unfortunately, eq A4 has the inverse dependence between b and ΔE.

The correct dependence is obtained by noting that the energy tied up in angular momentum conservation must be left in relative translation, i.e., $\Delta E_{min} = E(b/d)^2$. The assumption we now make to generalize this result is that the energy left in translation and unavailable to induce fragmentation is a function of this energy, i.e., $\Delta E = \Delta E_{min}^{1/n} = [E(b/d)^2]^{1/n}$ or $b^2 = d^2\Delta E^n/E$. Following the derivation of our previous work, we replace the integration over b in eq A2 by an integration over ΔE. To do this, we differentiate the expression for b^2 to obtain

$$d(b^2) = 2b\, db = nd^2\Delta E^{n-1}/E\, d(\Delta E) \qquad (A5)$$

Finally, we identify $\Omega(E)$ as the probability that dissociation occurs at a given value of b (or ΔE) and E. As defined above, the internal energy of the cluster is $E_T - \Delta E$, such that the RRKM rate constant for dissociation is given by $k(E_T - \Delta E - E_0)$ in the form of eq A1. Because the time available for dissociation is τ, the probability for dissociation is

$$\Omega(E) = 1 - \exp[-k(E_T - \Delta E - E_0)\tau] \qquad (A6)$$

Substituting eqs A5 and A6 into eq A2 yields

$$\sigma(E) = (n\sigma_0/E)\int_0^{E_T - E_0} (\Delta E)^{n-1}[1 - \exp\{-k(E_T - \Delta E - E_0)\tau\}]\, d(\Delta E) \qquad (A7)$$

This cross section is a convolution of the empirical form of eq 4 with the RRKM probability for dissociation on a time scale τ. As for the form previously suggested, eq A7 reverts to the empirical form of eq 4 when the rate constant is high. This property of eq A7 is a primary justification for the assumption made to obtain eq A5.

Equation A7 differs from the form previously suggested, eq A7 of ref 48, only by the term ΔE^{n-1}, which replaces $(E_T - \Delta E - E_0)^{n-1}$. Extensive comparisons of data analysis with these two equations yield very similar results for both metal cluster and metal carbonyl ion systems. In all cases, any differences are smaller than the cited error limits. The reasons for this are straightforward to understand. Both equations revert to the empirical form of eq 4, and therefore have the same fundamental energy dependence for the cross section. In essence, the only difference is in the weighting of the RRKM dissociation probabilities represented by the ΔE^{n-1} vs the $(E_T - \Delta E - E_0)^{n-1}$ terms. When the lifetime effect is small, then the different weighting cannot have a large effect on the threshold determined and when the lifetime effect is large, it is the dissociation probability term, $1 - \exp[-k\tau]$, that dominates the location of the threshold. Because neither implementation of the lifetime effect is rigorously derived, we have chosen to use both expressions and report the average result, including the difference in the results obtained with the two equations as part of the reported errors.

In its present application, the primary difficulty in applying eq A7 to the analysis of experimental data is that three numerical integrations are required to yield the model cross sections for comparison to the data: the integration over the dissociation probability in eq A7, the summation over internal energies (implicitly contained in the E_T term of eq A7 and shown explicitly in eq 4), and the integration over the translational energy distributions described elsewhere.[27] Although this makes data analysis time consuming, it is nevertheless straightforward.

References and Notes

(1) See, for example: Cotton, F. A.; Wilkinson, G. *Advanced Inorganic Chemistry*, 5th ed.; John Wiley and Sons: New York, 1988. Huheey, J. E. *Inorganic Chemistry: Principles of Structure and Reactivity*, 3rd ed.; Harper and Row: New York, 1983.

(2) Hoffmann, R. *Angew. Chem., Intl. Ed. Engl.* **1982**, *21*, 711.

(3) Schultz, R. H.; Crellin, K. C.; Armentrout, P. B. *J. Am. Chem. Soc.* **1991**, *113*, 8590.

(4) Dearden, D. V.; Hayashibara, K.; Beauchamp, J. L.; Kirchner, N. J.; van Koppen, P. A. M.; Bowers, M. T. *J. Am. Chem. Soc.* **1989**, *111*, 2401.

(5) Representative examples are: Winters, R. E.; Kiser, R. W. *Inorg. Chem.* **1964**, *3*, 699. Distefano, G. *J. Res. Natl. Bur. Stand., Sect. A* **1970**, *74*, 233.

(6) Representative examples are: Bach, S. B. H.; Taylor, C. A.; Van Zee, R. J.; Vala, M. T.; Weltner, W., Jr. *J. Am. Chem. Soc.* **1986**, *108*, 7104. Ray, U.; Brandow, S. L.; Bandukwalla, G.; Venkataraman, B.; Zhang, Z.;

Vernon, M. *J. Chem. Phys.* **1988**, *89*, 4092. McQuaid, M. J.; Morris, K.; Gole, J. L. *J. Am. Chem. Soc.* **1988**, *110*, 5280. Venkataraman, B.; Hou, H.; Zhang, Z.; Chen, S.; Bandukwalla, G.; Vernon, M. *J. Chem. Phys.* **1990**, *92*, 5338. Rayner, D. M.; Ishikawa, Y.; Brown, C. E.; Hackett, P. A. *J. Chem. Phys.* **1991**, *94*, 5471.

(7) Fletcher, T. R.; Rosenfeld, R. N. *J. Am. Chem. Soc.* **1988**, *110*, 2097.

(8) Representative examples are: Stevens, A. E.; Feigerle, C. S.; Lineberger, W. C. *J. Am. Chem. Soc.* **1982**, *104*, 5026. Sunderlin, L. S.; Wang, D.; Squires, R. R. *J. Am. Chem. Soc.* **1992**, *114*, 2788; submitted for publication.

(9) Barnes, L. A.; Rosi, M.; Bauschlicher, C. W., Jr. *J. Chem. Phys.* **1990**, *93*, 609.

(10) Mavridis, A.; Harrison, J. F.; Allison, J. *J. Am. Chem. Soc.* **1989**, *111*, 2482.

(11) Winters, R. E.; Kiser, R. W. *Inorg. Chem.* **1965**, *4*, 157.

(12) Foffani, A.; Pignataro, S.; Cantone, B.; Grasso, F. *Z. Phys. Chem.* **1965**, *45*, 79.

(13) Bidinosti, D. R.; McIntyre, N. S. *Can. J. Chem.* **1967**, *45*, 641.

(14) Junk, G. A.; Svec, H. J. *Z. Naturforsch. B* **1968**, *23*, 1.

(15) Michels, G. D.; Flesch, G. D.; Svec, H. J. *Inorg. Chem.* **1980**, *19*, 479.

(16) Das, P. R.; Nishimura, T.; Meisels, G. G. *J. Phys. Chem.* **1985**, *89*, 2808.

(17) Cox, J. D.; Pilcher, G. *Thermochemistry of Organic and Organometallic Compounds*; Academic Press: London, 1970.

(18) Cotton, F. A.; Fischer, A. K.; Wilkinson, G. *J. Am. Chem. Soc.* **1956**, *78*, 5168.

(19) Rosenstock, H. M.; Draxl, K.; Steiner, B. W.; Herron, J. T. *J. Phys. Chem. Ref. Data* **1977**, *6*, Suppl. No. 1.

(20) Connor, J. A.; Skinner, H. A.; Virmani, Y. *J. Chem. Soc., Faraday Trans. 1* **1972**, *68*, 1754.

(21) Pittam, D. A.; Pilcher, G.; Barnes, D. S.; Skinner, H. A.; Todd, D. *J. Less-Common Metals* **1975**, *42*, 217.

(22) Pilcher, G.; Ware, M. J.; Pittam, D. A. *J. Less-Common Metals* **1975**, *42*, 223.

(23) Lias, S. G.; Bartmess, J. E.; Liebman, J. F.; Holmes, J. L.; Levin, R. D.; Mallard, W. G. *J. Phys. Chem. Ref. Data* **1988**, *17*, Suppl. No. 1.

(24) Chase, M. W.; Davies, C. A.; Downey, J. R.; Frurip, D. J.; McDonald, R. A.; Syverud, A. N. *J. Phys. Chem. Ref. Data* **1985**, *14*, Suppl. No. 1.

(25) Shimanouchi, T. *J. Phys. Chem. Ref. Data* **1977**, *6*, 1095.

(26) Lloyd, D. R.; Schlag, E. W. *Inorg. Chem.* **1969**, *8*, 2544.

(27) Ervin, K. M.; Armentrout, P. B. *J. Chem. Phys.* **1985**, *83*, 166.

(28) Schultz, R. H.; Armentrout, P. B. *Int. J. Mass Spectrom. Ion Processes* **1991**, *107*, 29.

(29) Fisher, E. R.; Armentrout, P. B. *J. Chem. Phys.* **1991**, *94*, 1150.

(30) Fisher, E. R.; Kickel, B. L.; Armentrout, P. B. *J. Chem. Phys.* **1992**, *97*, 4859.

(31) Hales, D. A.; Lian, L.; Armentrout, P. B. *Int. J. Mass Spectrom. Ion Processes* **1990**, *102*, 269.

(32) Beyer, T.; Swinehart, D. F. *Comm. Assoc. Comput. Machines* **1973**, *16*, 379. Stein, S. E.; Rabinovitch, B. S. *J. Chem. Phys.* **1973**, *58*, 2438; *Chem. Phys. Lett.* **1977**, *49*, 183. Gilbert, R. G.; Smith, S. C. *Theory of Unimolecular and Recombination Reactions*; Blackwell Scientific: Oxford, U.K., 1990.

(33) Weber, M. E.; Elkind, J. L.; Armentrout, P. B. *J. Chem. Phys.* **1986**, *84*, 1521.

(34) Armentrout, P. B.; Simons, J. *J. Am. Chem. Soc.* **1992**, *114*, 8627.

(35) Magnera, T. F.; David, D. E.; Stulik, D.; Orth, R. G.; Jonkman, H. T.; Michl, J. *J. Am. Chem. Soc.* **1989**, *111*, 5036.

(36) Yu, W.; Liang, X.; Freas, R. B. *J. Phys. Chem.* **1991**, *95*, 3600.

(37) Aristov, N.; Armentrout, P. B. *J. Phys. Chem.* **1986**, *90*, 5135.

(38) Sugar, J.; Corliss, C. *J. Phys. Chem. Ref. Data* **1985**, *14*, Suppl. No. 2.

(39) Lessen, D. E.; Asher, R. L.; Brucat, P. J. *Chem. Phys. Lett.* **1991**, *177*, 380.

(40) Partridge, H.; Bauschlicher, C. W., Jr.; Langhoff, S. R. *J. Phys. Chem.* **1992**, *96*, 5350.

(41) Schultz, R. H.; Armentrout, P. B. *J. Phys. Chem.* **1993**, *97*, 596.

(42) Rothe, E. W.; Bernstein, R. B. *J. Chem. Phys.* **1959**, *31*, 1619.

(43) Lessen, D.; Brucat, P. J. *J. Chem. Phys.* **1989**, *91*, 4522.

(44) Bauschlicher, C. W., Jr.; Partridge, H.; Langhoff, S. R. *J. Chem. Phys.* **1989**, *91*, 4733.

(45) Bauschlicher, C. W., Jr.; Langhoff, S. R. *Int. Rev. Phys. Chem.* **1990**, *9*, 149. Bauschlicher, C. W., Jr.; Partridge, H.; Langhoff, S. R. In *Advances in Metal and Semiconductor Clusters*; Duncan, M. A., Ed.; JAI: Greenwich, CT; in press.

(46) Cotton, F. A.; Fischer, A. K.; Wilkinson, G. *J. Am. Chem. Soc.* **1959**, *81*, 800.

(47) Huber, M. C. E.; Sandeman, R. J.; Tubbs, E. F. *J. Phys. Chem. Ref. Data* **1985**, *14*, 264.

(48) Loh, S. K.; Hales, D. A.; Lian, L.; Armentrout, P. B. *J. Chem. Phys.* **1989**, *90*, 5466.

(49) Hales, D. A.; Lian, L.; Armentrout, P. B. *Int. J. Mass Spectrom. Ion Processes* **1990**, *102*, 269. Lian, L.; Su, C.-X.; Armentrout, P. B. *J. Chem. Phys.* **1992**, *96*, 7542; **1992**, *97*, 4072, 4084.

(50) Armentrout, P. B.; Hales, D. A.; Lian, L. In *Advances in Metal and Semiconductor Clusters*; Duncan, M. A., Ed.; JAI: Greenwich, CT; Vol. II, in press.

(51) (a) Seder, T. A.; Church, S. P.; Ouderkirk, A. J.; Weitz, E. *J. Am. Chem. Soc.* **1985**, *107*, 1432. (b) Seder, T. A.; Church, S. P.; Weitz, E. *J. Am. Chem. Soc.* **1986**, *108*, 4721.

(52) Fletcher, T. R.; Rosenfeld, R. N. *J. Am. Chem. Soc.* **1985**, *107*, 2203; **1986**, *108*, 1686.

(53) Seder, T. A.; Ouderkirk, A. J.; Weitz, E. *J. Chem. Phys.* **1986**, *85*, 1977.

(54) Elian, M.; Hoffmann, R. *Inorg. Chem.* **1975**, *14*, 1058.

(55) Burdett, J. K. *J. Chem. Soc., Faraday Trans. 2* **1974**, *70*, 1599.

(56) Carter, E. A.; Goddard, W. A., III *J. Phys. Chem.* **1988**, *92*, 5679.

(57) Griffith, J. S. *J. Inorg. Nucl. Chem.* **1956**, *2*, 1, 229.

(58) Catalan, M. A.; Rohrlich, F.; Shenstone, A. G. *Proc. R. Soc.* **1954**, *A221*, 421.

(59) Khan, F. A.; Steele, D. L.; Armentrout, P. B., unpublished results.

(60) Elian and Hoffmann calculate that $M(CO)_4$ with five d electrons has an optimum geometry that is C_{2v} with $\phi = 100°$ and $\phi' = 160°$, Figure 9, but do not provide the orbital energies for this particular geometry. We approximate the orbital energies by referring to two related geometries, namely C_{2v} ($\phi = 100°$ and $\phi' = 180°$) and D_{2d} ($\tau = 130°$), Figure 9, for which the orbital energies have been calculated.

(61) Armentrout, P. B. In *Advances in Gas Phase Ion Chemistry*; Adams, N. G., Babcock, L. M., Eds.; JAI: Greenwich, CT, 1992; Vol. 1, pp 83–119.

(62) Robinson, P. J.; Holbrook, K. A. *Unimolecular Reactions*; Wiley-Interscience: New York, 1972.

(63) Waage, E. V.; Rabinovitch, B. S. *Chem. Rev.* **1970**, *70*, 377.

(64) Based on the data of Whitaker, A.; Jeffrey, J. W. *Acta Crystallogr.* **1967**, *23*, 977.

(65) Levine, R. D.; Bernstein, R. B. *Molecular Reaction Dynamics and Chemical Reactivity*; Oxford University Press: New York, 1987; pp 59–60.

(66) Armentrout, P. B.; Beauchamp, J. L. *J. Chem. Phys.* **1981**, *74*, 2819.

(67) Aristov, N.; Armentrout, P. B. *J. Am. Chem. Soc.* **1986**, *108*, 1806.